

Josephson vortices and intrinsic Josephson junctions in the layered iron-based superconductor $Ca_{10}(Pt_3As_8)((Fe_{0.9}Pt_{0.1})_2As_2))_5$

Qiang-Tao Sui(随强涛), and Xiang-Gang Qui(邱祥冈)
Citation: Chin. Phys. B, 2022, 31 (**9**): 097403. DOI: 10.1088/1674-1056/ac76ae
Journal homepage: http://cpb.iphy.ac.cn; http://iopscience.iop.org/cpb

What follows is a list of articles you may be interested in

Raman phonon anomalies in $Sr(Fe_{1-x}Co_x)_2As_2$

Yanxing Yang(杨彦兴), Hewei Zhang(张鹤巍), and Haizheng Zhuang(庄海正)
Chin. Phys. B, 2022, 31 (**2**): 027401. DOI: 10.1088/1674-1056/ac0cd6

Superconductivity in octagraphene

Jun Li(李军) and Dao-Xin Yao(姚道新)
Chin. Phys. B, 2022, 31 (**1**): 017403. DOI: 10.1088/1674-1056/ac40fa

Dispersion of neutron spin resonance mode in $Ba_{0.67}K_{0.33}Fe_2As_2$

Tao Xie(谢涛), Chang Liu(刘畅), Tom Fennell, Uwe Stuhr, Shi-Liang Li(李世亮), and Hui-Qian Luo(罗会仟)
Chin. Phys. B, 2021, 30 (**12**): 127402. DOI: 10.1088/1674-1056/ac3651

Revealing the A_{1g}-type strain effect on superconductivity and nematicity in FeSe thin flake

Zhaohui Cheng(程朝晖), Bin Lei(雷彬), Xigang Luo(罗习刚), Jianjun Ying(应剑俊), Zhenyu Wang(王震宇), Tao Wu(吴涛), and Xianhui Chen(陈仙辉)
Chin. Phys. B, 2021, 30 (**9**): 097403. DOI: 10.1088/1674-1056/ac1efa

Nodal superconducting gap in LiFeP revealed by NMR: Contrast with LiFeAs

A F Fang(房爱芳), R Zhou(周睿), H Tukada, J Yang(杨杰), Z Deng(邓正), X C Wang(望贤成) , C Q Jin(靳常青), and Guo-Qing Zheng(郑国庆)
Chin. Phys. B, 2021, 30 (**4**): 047403. DOI: 10.1088/1674-1056/abec37

RAPID COMMUNICATION

Josephson vortices and intrinsic Josephson junctions in the layered iron-based superconductor $Ca_{10}(Pt_3As_8)((Fe_{0.9}Pt_{0.1})_2As_2)_5$

Qiang-Tao Sui(随强涛)[1,2] and Xiang-Gang Qui(邱祥冈)[1,2,3,†]

[1] *Beijing National Laboratory for Condensed Matter Physics, Institute of Physics, Chinese Academy of Sciences, Beijing* 100190, *China*
[2] *School of Physical Sciences, University of Chinese Academy of Sciences, Beijing* 100049, *China*
[3] *Songshan Lake Materials Laboratory, Dongguan* 523808, *China*

(Received 12 May 2022; revised manuscript received 31 May 2022; accepted manuscript online 8 June 2022)

Modulated electronic state due to the layered crystal structures brings about moderate anisotropy of superconductivity in the iron-based superconductors and thus Abrikosov vortices are expected in the mixed state. However, based on the angular and temperature dependent transport measurements in iron-based superconductor $Ca_{10}(Pt_3As_8)((Fe_{0.9}Pt_{0.1})_2As_2)_5$ with $T_c \simeq 12$ K, we find clear evidences of a crossover from Abrikosov vortices to Josephson vortices at a crossover temperature $T^\star \simeq 7$ K, when the applied magnetic field is parallel to the superconducting FeAs layers, i.e., the angle between the magnetic field and the FeAs layers $\theta = 0^\circ$. This crossover to Josephson vortices is demonstrated by an abnormal decrease (increase) of the critical current (flux-flow resistance) below $T^\star$, in contrast to the increase (decrease) of the critical current (flux-flow resistance) above $T^\star$ expected for Abrikosov vortices. Furthermore, when θ is larger than 0.5°, the flux-flow resistance and critical current have no anomalous behaviors across $T^\star$. These anomalous behaviors can be understood in terms of the distinct transition from the well-pinned Abrikosov vortices to the weakly-pinned Josephson vortices upon cooling, when the coherent length perpendicular to the FeAs layers $\xi_\perp$ becomes shorter than half of the interlayer distance $d/2$. These experimental findings indicate the existence of intrinsic Josephson junctions below $T^\star$ and thus quasi-two-dimensional superconductivity in $Ca_{10}(Pt_3As_8)((Fe_{0.9}Pt_{0.1})_2As_2)_5$, similar to those in the cuprate superconductors.

Keywords: iron-based superconductor, Abrikosov vortices, Josephson vortices, intrinsic Josephson junctions

PACS: 74.70.Dd, 74.25.Ha, 74.81.Fa **DOI:** 10.1088/1674-1056/ac76ae

1. Introduction

Nowadays the well-known applications based on Josephson junctions, such as superconducting quantum interference device (SQUID), superconducting qubit,[1–4] single-photon detector[5] and ac Josephson junction laser,[6] have demonstrated the possibility of potential large scale applications of superconductivity. In contrast to Josephson junctions made up of artificial superconducting heterostructures, the intrinsic Josephson junctions (iJJs)[7–13] formed inside single crystals possess atomic flatness and fewer defects, and provide unique applications, e.g., THz sources. In high-T_c cuprate superconductors, measurements of dc and ac Josephson effects[7,8,12–18] indicate that iJJs are formed between CuO_2 superconducting layers, which provide direct evidence for alternating stacks of superconducting and non-superconducting layers. For anisotropic layered superconductors, the coherent length normal to the superconducting layers $\xi_\perp$ and the interlayer distance d are two characteristic lengths that play a crucial role in determining the distribution of out-of-plane superconducting order parameter. Since $\xi_\perp$ decreases with lower temperature, a reasonable expectation of shorter $\xi_\perp$ is that Cooper pairs condense into the superconducting layers and a crossover from three-dimensional (3D) to quasi-two-dimensional (quasi-2D) superconductivity should occur at an intermediate temperature $T^\star$ when $\xi_\perp$ becomes shorter than $d/2$.[19] Accordingly, iJJs can be formed in the anisotropic layered superconductors, such as the case of cuprate superconductors.[7,8,12–18] Since the iron-based superconductors discovered in 2008[20–23] have similar layered structure with the cuprates, whose superconductivity is assumed to emerge in the FeAs or FeSe layers,[24–28] a natural question to ask is whether iJJs are also formed in the iron-based superconductors or not.

For iJJs in a magnetic field parallel to the superconducting layers, there exist vortices in the form of Josephson vortices. Josephson vortices are free to flow along the superconducting layers driven by the current perpendicular to the superconducting layers, due to the fact that the cores of Josephson vortices are phase cores formed between the superconducting layers and thus the pinning effect of defects on Josephson vortices is weak.[29,30] In contrary to Josephson vortices, Abrikosov vortices suffer from strong pinning of defects due to their normal state cores. Consequently, the Abrikosov vortices flow is susceptible to the temperature because pinning of defects gets stronger upon cooling, e.g., in the iron-based superconductors.[31,32] When the magnetic field slightly deviates from the superconducting layers, the Josephson vortices flow is affected by the strong pinning of Abrikosov vortices

†Corresponding author. E-mail: xgqiu@iphy.ac.cn

© 2022 Chinese Physical Society and IOP Publishing Ltd

due to the formation of composite vortex structures.[33] Therefore, to reveal the existence of Josephson vortices by the different behaviors of Josephson and Abrikosov vortices, the formation of iJJs in anisotropic layered superconductors can be confirmed.

In the iron-based superconductors, c-axis transport measurements on SmFeAs(O, F), LaFeAs(O, F)[34] and $(V_2Sr_4O_6)Fe_2As_2$[35] as well as torque measurements on $LaO_{0.9}F_{0.1}FeAs$ and $SmO_{0.9}F_{0.1}FeAs$[36] have suggested the existence of Josephson vortices. It is of great interest to explore the possibility of intrinsic Josephson junction behavior in other iron-based superconductors. In this work, by using the angular and temperature dependent transport measurements, we investigated the vortex dynamics of the iron-based superconductor single crystal $Ca_{10}(Pt_3As_8)((Fe_{0.9}Pt_{0.1})_2As_2)_5$ with $T_c \simeq 12$ K. Our results show that the behaviors of flux flow present a remarkable change at a crossover temperature $T^\star \simeq 7$ K, which indicates the distinct transition of the intrinsic structure of the vortices from the well-pinned Abrikosov vortices above $T^\star$ to the weakly-pinned Josephson vortices below $T^\star$, suggesting the existence of Josephson vortices and the formation of iJJs in $Ca_{10}(Pt_3As_8)((Fe_{0.9}Pt_{0.1})_2As_2)_5$.

2. Experimental details

The $Ca_{10}(Pt_3As_8)((Fe_{0.9}Pt_{0.1})_2As_2)_5$ single crystals were grown using the self-flux method, as described elsewhere.[37,38] The crystal structure was characterized by x-ray diffraction (RigakuD/MAX-Ultima III) using Cu K_α radiation ($\lambda = 0.154$ nm) at room temperature. Magnetization measurements were done using a superconducting quantum interference device (SQUID-VSM, Quantum Design). Transport measurements were performed in a physical property measurement system (PPMS-9, Quantum Design), which was connected to an external digital lock-in amplifier (SR830). In order to apply the current perpendicular to the FeAs layers, the samples were microfabricated with the focused ion beam (FIB) technique. Details of this process on FIB sample preparation have been reported elsewhere.[39] The samples connected to a puck were mounted on a PPMS horizontal rotator to scan θ at a resolution of 0.015°.

3. Results and discussion

3.1. Results

Figure 1(a) shows the x-ray diffraction (XRD) result of the $Ca_{10}(Pt_3As_8)((Fe_{0.9}Pt_{0.1})_2As_2)_5$ single crystals. All of the indexed peaks identified belong to the $Ca_{10}(Pt_3As_8)(Fe_2As_2)_5$ triclinic structure phase. The presence of only $(00l)$ reflection peaks indicates that the natural cleavage planes are parallel to the FeAs layers and the stacks of alternating FeAs and PtAs layers are perfect. The calculated interlayer distance is $d \sim 10.283$ Å, close to the previous reported value.[37] The temperature-dependent resistivity $\rho_{ab}(T)$ shows that as the temperature is lowered, the metallic behavior is followed by a semiconducting one, and finally superconductivity emerges below 12.8 K as shown in Fig. 1(b). The bulk superconductivity is confirmed by the diamagnetic signal observed in both zero-field-cooling (ZFC) and field-cooling (FC) measurements below 12.4 K, which is consistent with that in the temperature-dependent resistivity $\rho_{ab}(T)$ measurements, as shown in Fig. 1(c).

To investigate the possible iJJs behaviors, we have measured the angular and temperature dependent resistance of the micro-fabricated sample with a cross-section of 2.5×1.9 μm^2 fabreicated by FIB technique as shown in Fig. 2(a). Upon cooling, the temperature-dependent resistivity $\rho_{c^*}(T)$ exhibits a semiconducting behavior above 15 K in the normal state, in contrast to that in Fig. 1(b), suggesting a weak coupling between the FeAs layers. From the angular dependent flux-flow resistance in Fig. 2(c), it can be seen that the flux-flow resistance overall decreases with lower temperature, which is consistent with the behaviors of Abrikosov vortices due to the enhanced pinning upon cooling. However, there exists a surprising exception in a narrow angular

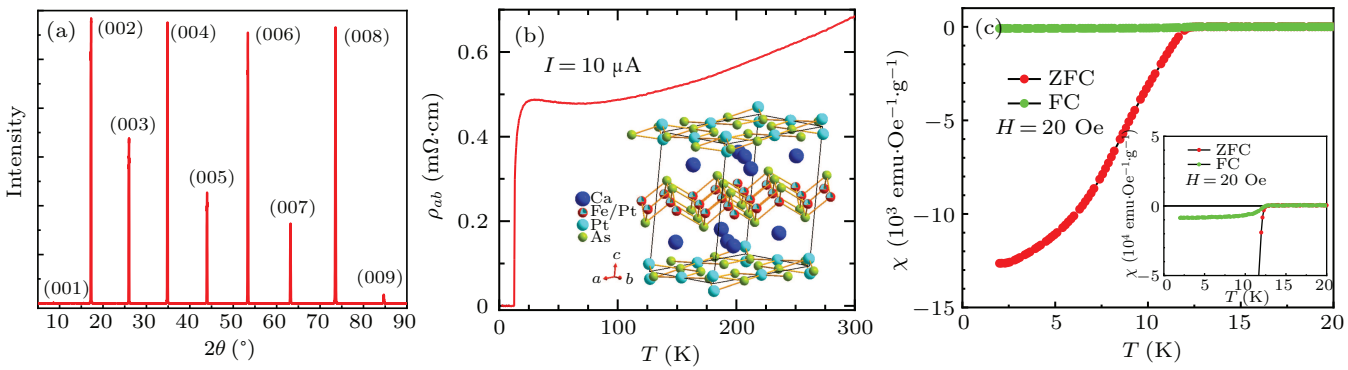


Fig. 1. The characterization of $Ca_{10}(Pt_3As_8)((Fe_{0.9}Pt_{0.1})_2As_2)_5$ single crystals. (a) The typical XRD θ–2θ scan of a $Ca_{10}(Pt_3As_8)((Fe_{0.9}Pt_{0.1})_2As_2)_5$ single crystal. (b) The temperature-dependent resistivity $\rho_{ab}(T)$ with the current $I = 10$ μA parallel to the FeAs layers. The inset is the schematic of the crystal structure of $Ca_{10}(Pt_3As_8)((Fe_{0.9}Pt_{0.1})_2As_2)_5$. (c) The temperature dependence of magnetic susceptibility measured in the zero field cooling (ZFC) and field cooling (FC) with the magnetic field $H = 20$ Oe parallel to the FeAs layers in order to weaken the demagnetization effect. The inset is the blowup of the temperature-dependent magnetic susceptibility near zero.

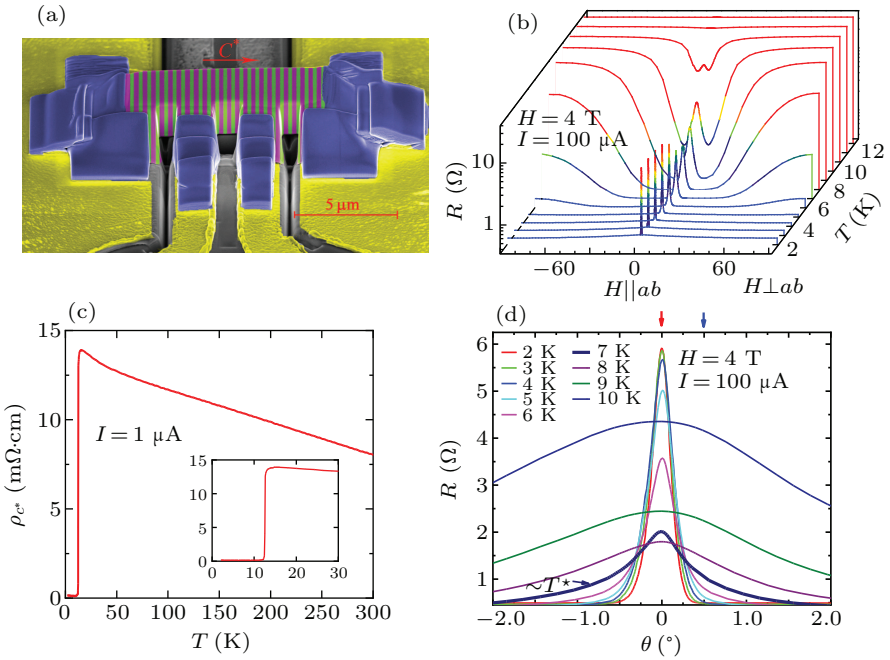


Fig. 2. The interlayer dissipation resistance of a typical $Ca_{10}(Pt_3As_8)((Fe_{0.9}Pt_{0.1})_2As_2)_5$ sample. (a) False-color scanning electron micrograph of a typical sample microfabricated by FIB technique. The crystal (alternating purple and green) was carved with four electrodes, each of which was connected to the Au electrode (yellow) via FIB-assisted deposited Pt (blue). The interlayer transport measurements were performed by the current flowing along c^* normal to the FeAs layers (green) indicated by the red arrow. The scale bar is 5 μm. (b) The temperature-dependent resistivity $\rho_{c^*}(T)$ with the current $I = 1$ μA. The inset is the blowup of $\rho_{c^*}(T)$ from 2 K to 30 K. (c) The flux-flow resistance as a function of θ in a fixed field of $H = 4$ T for several temperatures. The current is $I = 100$ μA. (d) The enlarged angular dependent flux-flow resistance of (c) in a narrow angular region ($\pm 2°$) around the FeAs layers below 10 K. The red and blue arrows correspond to $\theta = 0°$ and $\theta = 0.5°$, respectively.

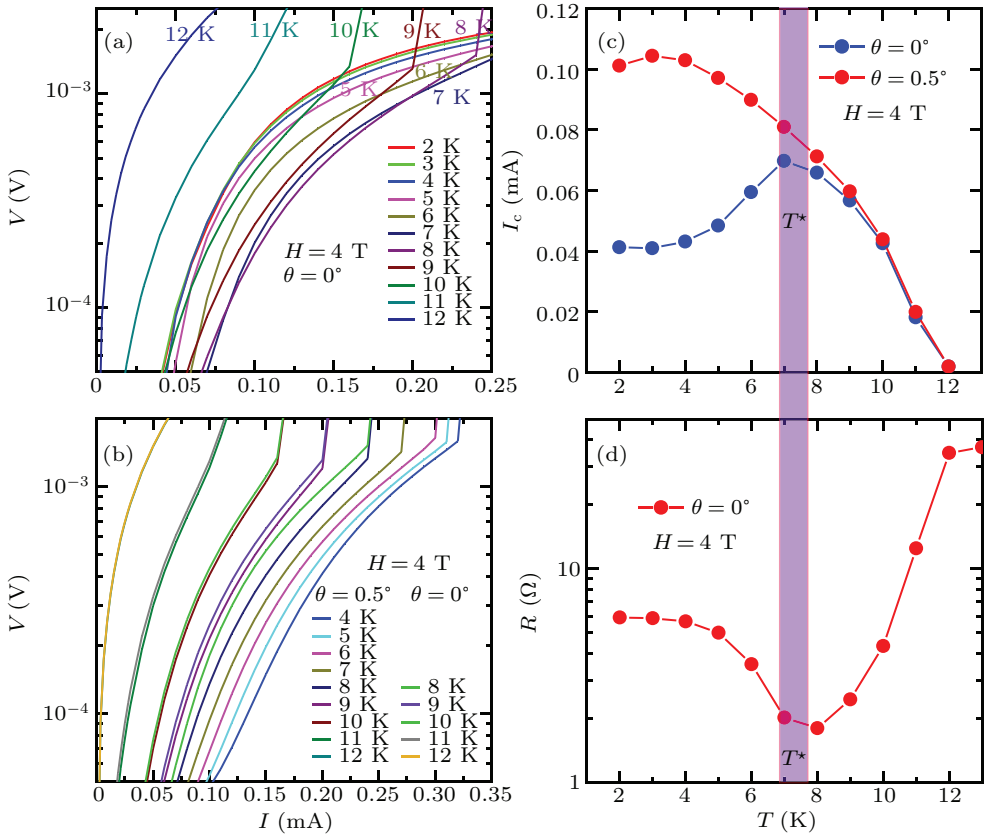


Fig. 3. The distinction of vortices dynamics behaviors below and above $T^\star$. (a) and (b) correspond to I–V curves at $\theta = 0°$ and $\theta = 0.5°$ in a fixed field of $H = 4$ T for several temperatures, respectively. $\theta = 0°$ and $\theta = 0.5°$ correspond to the angles marked by the red and blue arrows in Fig. 2(d), respectively. (c) The temperature dependence of the critical current extracted from (a) and (b). The voltage criterion of the critical current is 50 μV. (d) The temperature dependence of the flux-flow resistance at $\theta = 0°$ extracted from Fig. 2(c).

region around $\theta = 0°$. Upon cooling from T_c, near $\theta = 0°$, a broad peak grows gradually in a background. At the crossover temperature $T^\star \simeq 7$ K, the background disappears and a sharp peak centered at $\theta = 0°$ emerges in a very narrow angular region (less than $\pm 0.5°$).

Figure 2(d) is a finer scan of the flux-flow resistance in a narrow angular region ($\pm 2°$) around the FeAs layers for several temperatures below 10 K. In contrast to the behavior of the resistance peak above $T^\star$, below $T^\star$ the resistance peak at $\theta = 0°$ first increases with the decreasing temperature and finally reaches saturation at lower temperatures.

To further clarify the difference of the vortex dynamics in the two temperature regions below and above $T^\star$, we have measured the current–voltage (I–V) characteristics at $\theta = 0°$ and $\theta = 0.5°$. At $\theta = 0°$, as shown in Fig. 3(a), above $T^\star$ upon cooling, the I–V curves shift to the right (higher bias current) due to the increase of the critical current. However, upon further cooling below $T^\star$, the temperature dependence of the I–V curves is reversed from that above $T^\star$, i.e., the lower the temperature, the smaller the critical current. On the other hand, at $\theta = 0.5°$ shown in Fig. 3(b), upon cooling across $T^\star$, no such a reversal is observed. Accordingly, the I–V curves always shift to the right (higher bias current), indicating the continuous increase of the critical current. In addition, the I–V curves at $0.5°$ are similar to those at $0°$ above $T^\star$. The critical current extracted from Figs. 3(a) and 3(b) is shown in Fig. 3(c). It can be seen in Fig. 3(c) that at $\theta = 0°$, the critical current first increases with the decreasing temperature, then decreases at $T^\star$ and finally reaches saturation at lower temperatures, while at $\theta = 0.5°$, the critical current continuously increases. From the flux-flow resistance at $\theta = 0°$ in Fig. 3(d), it is confirmed that increase (decrease) of the flux-flow resistance corresponds to decrease (increase) of the critical current and a same crossover temperature $T^\star$ can be obtained.

3.2. Discussion

As the magnetic field is aligned parallel to the FeAs layers, the increase (decrease) of the critical current (flux-flow resistance) above $T^\star$ upon cooling, is consistent with what is expected for Abrikosov vortices under enhanced pinning as the temperature is lowered. However, the anomalous decrease (increase) of the critical current (flux-flow resistance) below $T^\star$ upon cooling, contradicts behaviors of Abrikosov vortices. These behaviors can be understood in terms of the change of superconducting order parameter perpendicular to the FeAs layers as the temperature is lowered. Above $T^\star$, owing to the larger $\xi_\perp$ than $d/2$, the superconducting order parameter is continuous and Abrikosov vortices are formed as shown in Fig. 4(a), which can be described by anisotropic Ginzburg–Landau model. However, below $T^\star$, $\xi_\perp$ gets shorter than $d/2$, resulting in the discrete superconducting order parameter perpendicular to the FeAs layers and Josephson vortices with phase cores, as shown in Fig. 4(b). In addition, as the magnetic field is deviated at a certain angle from the FeAs layers, the composite vortex structures are formed by connecting Josephson vortices to Abrikosov vortices below $T^\star$, as shown in Fig. 4(c). Therefore, due to the strong pinning of Abrikosov vortices, no anomaly of the flux-flow resistance and the critical current is found across $T^\star$. In $Bi_2Sr_2CaCu_2O_{8+\delta}$, such an increase in the angular dependent flux-flow resistance is identified as the behavior of the lock-in Josephson vortices,[29,30] which arises from iJJs formed inside $Bi_2Sr_2CaCu_2O_{8+\delta}$ due to the extremely short $\xi_\perp$. Therefore, the anomalous behaviors below $T^\star$ at $\theta = 0°$ can be a result of the formation of Josephson vortices in $Ca_{10}(Pt_3As_8)((Fe_{0.9}Pt_{0.1})_2As_2)_5$, which is associated with iJJs formed between the FeAs layers.

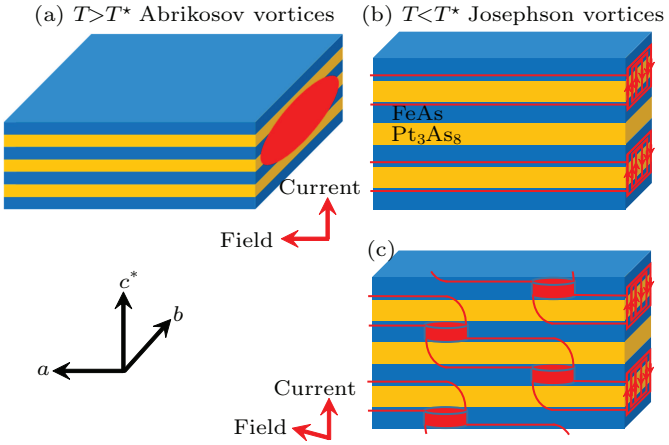


Fig. 4. The change in the intrinsic structures of the vortices. (a) and (b) correspond to Abrikosov vortices above $T^\star$ and Josephson vortices below $T^\star$ with the magnetic field aligned well along the FeAs layers and the current perpendicular to the FeAs layers, respectively. (c) The structures connecting Josephson vortices to Abrikosov vortices below $T^\star$, as the magnetic field is deviated at certain angle from the FeAs layers.

From the above physical scenario, the crossover from Abrikosov vortices to Josephson vortices upon cooling occurs when $\xi_\perp$ is equal to $d/2$. From XRD, we calculate the interlayer distance $d \sim 10.283$ Å. Using the Bardeen–Cooper–Schrieffer (BCS) relation $\xi_\perp(T) = \xi_\perp(0)/\sqrt{1 - T/T_c}$, it is found that $\xi_\perp(T^\star) = \xi_\perp(0)/\sqrt{1 - T^\star/T_c} = d/2$ and $\xi_\perp(0)$ is estimated to be 3.319 Å, which is smaller than 12 Å calculated from the upper critical magnetic field.[37] Moreover, chemical valence analysis demonstrates perfectly balanced charge in the Pt_3As_8 layers and thus the Pt_3As_8 layers do not contribute to the density of state at the Fermi level E_F,[37,40] which results in weak coupling between the FeAs layers and short $\xi_\perp(0)$.

There are two distinct physical origins for the flux-flow resistance and critical current above and blow $T^\star$ upon cooling. Above $T^\star$, vortices exist in the form of Abrikosov vortices. The increase (decrease) of the critical current (flux-flow resistance) originates from the enhanced pinning with the decreasing temperature. Below $T^\star$, the shorter $\xi_\perp$ with lower

temperature results in the thinner superconducting layers s and the thicker non-superconducting layers t. In order to determine the critical current (maximum supercurrent) carried by iJJs with N Josephson junctions in the magnetic field H, the spatial dependence of the gauge-invariant phase differences γ_n in the junction n need be derived. In the following, the junction length, the magnetic field H and the tunneling current are along x, y and z directions, respectively. The second spatial derivative equations[29,41,42] describing γ_n are

$$\frac{\mathrm{d}^2\gamma_n}{\mathrm{d}x^2} = \frac{1}{\lambda_\mathrm{J}^2}\sin\gamma_n - \frac{1}{\lambda_\mathrm{k}^2}(\sin\gamma_{n-1} + \sin\gamma_{n+1}),$$
$$n = 1,\ldots,N, \tag{1}$$

$$\lambda_\mathrm{J} = \sqrt{\frac{\Phi_0}{2\pi\mu_0 j_\mathrm{c}(t_\mathrm{eff} + \frac{2\lambda^2}{s_\mathrm{eff}})}}, \quad \lambda_\mathrm{k} = \sqrt{\frac{\Phi_0 s_\mathrm{eff}}{2\pi\mu_0 j_\mathrm{c}\lambda^2}}, \tag{2}$$

where λ is the London penetration depth for screening currents flowing in the FeAs layers, j_c is the tunneling current density, $s_\mathrm{eff} = \lambda\sinh(\frac{s}{\lambda})$ and $t_\mathrm{eff} = t + 2\lambda\tanh(\frac{s}{2\lambda})$. The second term on the right-hand side of Eq. (1) describes the coupling between the adjacent iJJs. Numerical simulation needs to be performed to solve Eq. (1). Based on the simulation results (Fig. 7 in Ref. [42]), we know the Meissner-effect response followed by Josephson vortices firstly penetrating into the middle junction. For simplicity, we consider the gauge-invariant phase screening effect only in the middle junction when the magnetic field is less than $H_\mathrm{c} = 16 j_\mathrm{c}\lambda_\mathrm{J}$.[43] H_c determines the critical current because the higher current makes the magnetic field greater than H_c so that Josephson vortices penetrate into the junction (a periodic gauge-invariant phase is established) resulting in no net supercurrent.

In $Ca_{10}(Pt_3As_8)((Fe_{0.9}Pt_{0.1})_2As_2)_5$, $\lambda \approx 1000$ nm[44] and $d = s + t \sim 10.283$ Å so that $s \ll \lambda$. For this limit, λ_k and λ_J are

$$\lambda_\mathrm{k} = \sqrt{\frac{\Phi_0 s}{2\pi\mu_0 j_\mathrm{c}\lambda^2}}, \tag{3}$$

$$\lambda_\mathrm{J} = \sqrt{\frac{\Phi_0}{2\pi\mu_0 j_\mathrm{c}(t + s + \frac{2\lambda^2}{s})}} = \sqrt{\frac{\Phi_0 s}{4\pi\mu_0 j_\mathrm{c}\lambda^2}} = \frac{\lambda_\mathrm{k}}{\sqrt{2}}. \tag{4}$$

In this case, we can get

$$H_\mathrm{c} = \sqrt{\frac{64\Phi_0 s j_\mathrm{c}}{\pi\mu_0\lambda^2}} = \frac{8\Phi_0 q^{\star 2}}{\pi m^\star}\sqrt{\frac{d-t}{2\zeta\sinh\frac{t}{\zeta}}}, \tag{5}$$

where $j_\mathrm{c} = \frac{q^\star\hbar}{m^\star\zeta\sinh(t/\zeta)}$ and $\zeta = \sqrt{\frac{\hbar^2}{2m^\star(\varepsilon_0 - V_0)}}$ is the characteristic length related to the energy ε_0 of the Cooper pair and the barrier potential V_0 of the non-superconducting layers. $q^\star$ and $m^\star$ are the effective charge and mass of the Cooper pair, respectively. Below $T^\star$, due to the smooth increase (from zero) of t upon cooling, H_c is reduced, which makes the critical current decrease and thus the flux-flow resistance increase at a fixed transport current above the critical current (consistent with smooth changes of both the critical current and flux-flow resistance in Figs. 3(c) and 3(d)).

4. Conclusion

In summary, a crossover from Abrikosov vortices to Josephson vortices at $T^\star \simeq 7$ K has been observed in the interlayer transport measurements in $Ca_{10}(Pt_3As_8)((Fe_{0.9}Pt_{0.1})_2As_2)_5$ with $T_\mathrm{c} \simeq 12$ K. Below $T^\star$, Josephson vortices are associated with the intrinsic Josephson junctions in $Ca_{10}(Pt_3As_8)((Fe_{0.9}Pt_{0.1})_2As_2)_5$. Our results demonstrate that the superconductivity is of quasi-2D nature in $Ca_{10}(Pt_3As_8)((Fe_{0.9}Pt_{0.1})_2As_2)_5$. It is of great interest to further explore the quasi-2D superconductivity in the iron-based superconductors from both fundamental and application points of view.

Acknowledgements

Project supported by the National Key Research and Development Program of China (Grant No. 2017YFA0302903) and the National Natural Science Foundation of China (Grant No. 11974412).

References

[1] Arute F, Arya K, Babbush R, *et al.* 2019 *Nature* **574** 505
[2] Place A P M, Rodgers L V H, Mundada P, *et al.* 2021 *Nat. Commun.* **12** 1779
[3] Wu Y L, Bao W S, Cao S R, *et al.* 2021 *Phys. Rev. Lett.* **127** 180501
[4] Ball P 2021 *Nature* **599** 542
[5] Walsh Evan D, Jung W, Lee G, Efetov Dmitri K, Wu B, Huang K F, Ohki Thomas, A, Taniguchi T, Watanabe K, Kim P, Englund D and Fong Kin C 2021 *Science* **372** 409
[6] Cassidy M C, Bruno A, Rubbert S, Irfan M, Kammhuber J, Schouten R N, Akhmerov A R and Kouwenhoven L P 2017 *Science* **355** 939
[7] Kleiner R, Steinmeyer F, Kunkel G and Müller P 1992 *Phys. Rev. Lett.* **68** 2394
[8] Rapp M, Murk A, Semerad R and Prusseit W 1996 *Phys. Rev. Lett.* **77** 928
[9] Inomata K, Sato S, Nakajima K, Tanaka A, Takano Y, Wang H B, Nagao M, Hatano H and Kawabata S 2005 *Phys. Rev. Lett.* **95** 107005
[10] Jin X Y, Lisenfeld J, Koval Y, Lukashenko A, Ustinov A V and Müller P 2006 *Phys. Rev. Lett.* **96** 177003
[11] Li S X, Qiu W, Han S, Wei Y F, Zhu X B, Gu C Z, Zhao S P and Wang H B 2007 *Phys. Rev. Lett.* **99** 037002
[12] Kawae T, Nagao M, Takano Y, Wang H, Hatano T, Kim S and Yamashita T 2005 *Supercond. Sci. Technol.* **18** 1159
[13] Kubo Y, Tanaka T, Takahide Y, Ueda S, Okutsu T, Islam A T M N, Tanaka I and Takano Y 2008 *Phys. C* **468** 1922
[14] Wang H B, Wu P H and Yamashita T 2001 *Phys. Rev. Lett.* **87** 107002
[15] Wei Y F, Zhao S P, Zhu X B, Chen G H, Ren Y F, Yu H W, Yang Q S and Hu Y 2005 *Chin. Phys. Lett.* **22** 2051
[16] Zhu X B, Wei Y F, Zhao S P, Chen G H and Yang Q S 2004 *Chin. Phys.* **13** 529
[17] Ozyuzer L, Koshelev A E, Kurter C, Gopalsami N, Li Q, Tachiki M, Kadowaki K, Yamamoto T, Minami H, Yamaguchi H, Tachiki T, Gray KE, Kwok W K and Welp U 2007 *Science* **318** 1291
[18] Borodianskyi E A and Krasnov V M 2017 *Nat. Commun.* **8** 1742
[19] Farrell D E, Rice J P, Ginsberg D M and Liu J Z 1990 *Phys. Rev. Lett.* **64** 1573
[20] Kamihara Y, Watanabe T, Hirano M and Hosono H 2008 *J. Am. Chem. Soc.* **130** 3296
[21] Matsuishi S, Inoue Y, Nomura T, Yanagi H, Hirano M and Hosono H 2008 *J. Am. Chem. Soc.* **130** 14428

[22] Chen X H, Wu T, Wu G, Liu R H, Chen H and Fang D F 2008 *Nature* **453** 761

[23] Ren Z A, Lu W, Yang J, Yi W, Shen X L, Cai Z, Che G C, Dong X L, Sun L L, Zhou F and Zhao Z X 2008 *Chin. Phys. Lett.* **25** 2215

[24] Raghu S, Qi X L, Liu C X, Scalapino D J and Zhang S C 2008 *Phys. Rev. B* **77** 220503

[25] Kuroki K, Onari S, Arita R, Usui H, Tanaka Y, Kontani H and Aoki H 2008 *Phys. Rev. Lett.* **101** 087004

[26] Lee P A and Wen X G 2008 *Phys. Rev. B* **78** 144517

[27] Ma F J, Lu Z Y and Xiang T 2008 *Phys. Rev. B* **78** 224517

[28] Ma F J, Lu Z Y and Xiang T 2010 *Frontiers of Physics in China* **5** 150

[29] Hechtfischer G, Kleiner R, Schlenga K, Walkenhorst W, Müller P and Johnson H L 1997 *Phys. Rev. B* **55** 14638

[30] Kadowaki K, Kakeya I, Yamamoto T, Yamazaki T, Kohri M and Kubo Y 2006 *Phys. C* **437–438** 111

[31] van der Beek C J, Rizza G, Konczykowski M, Fertey P, Monnet I, Klein T, Okazaki R, Ishikado M, Kito H, Iyo A, Eisaki H, Shamoto S, Tillman M E, Bud'ko SL, Canfield P C, Shibauchi T and Matsuda Y 2010 *Phys. Rev. B* **81** 174517

[32] Yamamoto A, Jaroszynski J, Tarantini C, Balicas L, Jiang J, Gurevich A, Larbalestier D C, Jin R, Sefat A S, McGuire M A, Sales B C, Christen D K and Mandrus D 2009 *Appl. Phys. Lett.* **94** 062511

[33] Blatter G, Feigel'man M V, Geshkenbein V B, Larkin A I and Vinokur V M 1994 *Rev. Mod. Phys.* **66** 1125

[34] Moll P J W, Balicas L, Geshkenbein V, Blatter G, Karpinski J, Zhigadlo N D and Batlogg B 2012 *Nat. Mater.* **12** 134

[35] Moll P J W, Zhu X, Cheng P, Wen H H and Batlogg B 2014 *Nat. Phys.* **10** 644

[36] Li G, Grissonnanche G, Conner B S, Wolff-Fabris F, Putzke C, Zhigadlo N D, Katrych S, Bukowski Z, Karpinski J and Balicas L 2013 *Phys. Rev. B* **87** 100503

[37] Ni N, Allred J M, Chan B C and Cava R J 2011 *Proc. Natl. Acad. Sci. USA* **108** E1019

[38] Kakiya S, Kudo K, Nishikubo Y, Oku K, Nishibori E, Sawa H, Yamamoto T, Nozaka T, Nohara M 2011 *J. Phys. Soc. Jpn.* **80** 093704

[39] Moll P J W, Puzniak R, Balakirev F, Rogacki K, Karpinski J, Zhigadlo N D and Batlogg B 2010 *Nat. Mater.* **9** 628

[40] Stürzer T, Derondeau G and Johrendt D 2012 *Phys. Rev. B* **86** 060516

[41] Sakai S, Bodin P and Pedersen N F 1993 *J. Appl. Phys.* **73** 2411

[42] Kleiner R, Müller P, Kohlstedt H, Pedersen N F and Sakai S 1994 *Phys. Rev. B* **50** 3942

[43] Tinkham M 2004 *Introduction to Superconductivity*, Dover edn. (New York: Dover Publications) pp. 215–220

[44] Kim J, Ronning F, Haberkorn N, Civale L, Nazaretski E, Ni N, Cava R J, Thompson J D and Movshovich R 2012 *Phys. Rev. B* **85** 180504